

## Journal: NETWORK NEUROSCIENCE

---

### 1 RESEARCH

## 2 The impact of Parkinson's disease on striatal network connectivity and 3 cortico-striatal drive: an in-silico study

4 **Ilaria Carannante<sup>1</sup>, Martina Scolamiero<sup>2</sup>, J. J. Johannes Hjorth<sup>1</sup>, Alexander Kozlov<sup>1,3</sup>, Bo Bekkouche<sup>1</sup>, Lihao Guo<sup>1</sup>,**  
5 **Arvind Kumar<sup>1</sup>, Wojciech Chacholski<sup>2</sup>,**  
6 **and Jeanette Hellgren Kotaleski<sup>1,3</sup>**

7 <sup>1</sup>Department of Computer Science, KTH Royal Institute of Technology, Stockholm, Sweden

8 <sup>2</sup>Department of Mathematics, KTH Royal Institute of Technology, Stockholm, Sweden

9 <sup>3</sup>Department of Neuroscience, Karolinska Institutet, Stockholm, Sweden

10 **Keywords:** Parkinson's disease, Striatum, Computational modeling, Topological data analysis, Directed cliques, Network  
11 higher order connectivity, Neuronal degeneration model

## ABSTRACT

12 Striatum, the input stage of the basal ganglia, is important for sensory-motor integration, initiation and  
13 selection of behaviour, as well as reward learning. Striatum receives glutamatergic inputs from mainly  
14 cortex and thalamus. In rodents, the striatal projection neurons (SPNs), giving rise to the direct and the  
15 indirect pathway (dSPNs and iSPNs, respectively), account for 95% of the neurons and the remaining 5%  
16 are GABAergic and cholinergic interneurons. Interneuron axon terminals as well as local dSPN and iSPN  
17 axon collaterals form an intricate striatal network. Following chronic dopamine depletion as in  
18 Parkinson's disease (PD), both morphological and electrophysiological striatal neuronal features are  
19 altered. Our goal with this in-silico study is twofold: a) to predict and quantify how the intrastriatal  
20 network connectivity structure becomes altered as a consequence of the morphological changes reported  
21 at the single neuron level, and b) to investigate how the effective glutamate drive to the SPNs would need

22 to be altered to account for the activity level seen in SPNs during PD. In summary we find that the  
23 richness of the connectivity motifs is significantly decreased during PD, while at the same time a  
24 substantial enhancement of the effective glutamatergic drive to striatum is present.

## AUTHOR SUMMARY

25 This in-silico study predicts that the impact the neuronal morphological alterations have on the striatal  
26 microcircuit connectivity. We find that the richness in the topological striatal motifs is significantly  
27 reduced in Parkinson's disease, highlighting that just measuring the pairwise connectivity between  
28 neurons gives an incomplete description of network connectivity. Also we predict how the resulting  
29 electrophysiological changes of SPN excitability together with their reduced number of dendritic  
30 branches affect their response to the glutamate drive from cortex and thalamus. We find that the effective  
31 glutamatergic drive is likely significantly increased in PD, in accordance with the hyperglutamatergic  
32 hypothesis.

## INTRODUCTION

33 Parkinson's disease (PD) is a progressive neurodegenerative disease, debilitating motor and cognitive  
34 systems. The progressive and chronic loss of dopamine results in a variety of changes in the ongoing and  
35 stimulus evoked activity in the striatum, the input stage of the basal ganglia (Figure 1A) (Sharott,  
36 Vinciati, Nakamura, and Magill (2017), Ketzef et al. (2017), Filipović et al. (2019)), globus pallidus  
37 (Mallet et al. (2008), Raz, Vaadia, and Bergman (2000), Tachibana, Iwamuro, Kita, Takada, and Nambu  
38 (2011)) and subthalamic nucleus (Bergman, Wichmann, Karmon, and DeLong (1994)) in both  
39 non-human primate and rodent models.

40 These neural activity alterations are accompanied by major changes in the morphology of the striatal  
41 projection neurons (SPNs). Postmortem analysis of neostriatal tissue reveals significant degeneration of  
42 the SPN dendrites in PD patients compared to controls without a history of neurological or  
43 neuropsychiatric illness. Neurodegeneration leads to a reduction by almost half of the total dendritic  
44 length and average length of the terminal dendritic segments at the most advanced stage of PD (McNeill,  
45 Brown, Rafols, and Shoulson (1988)). Dendritic degeneration is more pronounced in the putamen than in  
46 the caudate nucleus and is particularly dramatic in the commissural and post-commissural regions where  
47 the total dendritic length is reduced to less than a quarter (Zaja-Milatovic et al. (2005)).

48 Rodent models have been used to understand striatal circuitry both in health and disease. SPNs  
49 account for about 95% of the neurons in the striatum in rodents and the remaining neurons are  
50 interneurons (Figure 1B). SPNs are equally divided into two subpopulations expressing D1 or D2  
51 dopamine receptors. The former, denoted dSPN, gives rise to the direct pathway and the latter, iSPN, the  
52 indirect pathway. In this computational study we have included the fast-spiking (FS), low threshold  
53 spiking (LTS) and cholinergic (ChIN) interneurons in addition to the two types of SPNs. Some  
54 neurotoxin-induced and genetic rodent models of Parkinson's disease are known to reproduce the  
55 dendritic degeneration dendritic degeneration of SPN, but the reduction of total dendritic length is not as  
56 dramatic as in human patients at the terminal stages of PD (for example: 6-OHDA model in Fieblinger et  
57 al. (2014), Fieblinger et al. (2018); aphakia model in Alberquilla, Gonzalez-Granillo, Martín, and  
58 Moratalla (2020); knockout D1R mice ( $D1R^{-/-}$ ) in Suarez, Solis, Sanz-Magro, Alberquilla, and  
59 Moratalla (2020)). Loss of SPN dendrites reduces both the SPN local connectivity (Taverna, Ilijic, and  
60 Surmeier (2008)) as well as the number of the glutamatergic synapses (Fieblinger et al. (2014), Zhai,

61 Shen, Graves, and Surmeier (2019)). In contrast to SPNs, fast spiking interneurons (FS) exhibit axonal  
62 sprouting (over 60% longer than in control) and formation of new functional FS synapses of similar  
63 strength specifically onto iSPNs. This rewiring of the local striatal network happens rapidly within the  
64 first week after the 6-OHDA lesion and precedes dendritic atrophy in SPNs (Gittis et al. (2011)).

65 Striatum is crucial for sensori-motor integration (Wall, De La Parra, Callaway, and Kreitzer (2013),  
66 de la Torre-Martinez, Ketzef, and Silberberg (2023)), action-selection (Redgrave, Prescott, and Gurney  
67 (1999)) and reinforcement learning (Doya (2008)). To better understand how these functions of the  
68 striatum are impaired by loss of dopamine it is important to characterise how changes in the neurons  
69 morphologies affect the network connectivity structure and representation of cortical and thalamic inputs.

70 To characterise how progressive loss of SPN dendrites and sprouting of FS axons impact network  
71 connectivity we use the digital reconstruction of the mouse striatal microcircuitry as in Hjorth et al.  
72 (2020). Here multi-compartmental neuron models capture both the morphological and  
73 electrophysiological features of the different neuron types. Network connectivity is then generated based  
74 on touch detection between dendrites and axons combined with pruning rules to match experimental  
75 connection probabilities (Figure 1C), as in previous studies of striatal (Hjorth et al. (2020)) and  
76 neocortical (Markram et al. (2015)) microcircuitry. In this in-silico microcircuit we systematically  
77 modify the neuron morphologies similarly to what is observed in Parkinson's disease and calculated not  
78 only the first order network properties (neuron degree and connection probability) but also the **directed**  
79 **cliques**. Directed cliques are structural feedforward motifs of all-to-all connected neurons which were  
80 recently used to capture higher order interactions in somatosensory cortex structural networks (Reimann  
81 et al. (2017)). In this study we found that progressive dendritic degeneration dramatically affects  
82 statistics of directed clique counts particularly at the later PD stages. Our analysis showed that  
83 interneurons (FS, LTS and ChIN), despite only accounting for 5% of the neurons, are key to the  
84 formation of high dimensional directed cliques. These results suggest that interneurons play a crucial role  
85 in shaping the striatal network structure.

86 Next, to understand how altered dendritic morphology and membrane properties influence the transfer  
87 of cortical inputs to the striatum we activated dSPN and iSPN with simulated cortical inputs and  
88 compared the control and the PD case. The SPN model parameters for the PD case were tuned to  
89 reproduce the electrophysiological changes observed in Fieblinger et al. (2014). We found that SPN loss  
90 of dendritic branches and glutamatergic input as seen in PD condition severely reduced neuron sensitivity

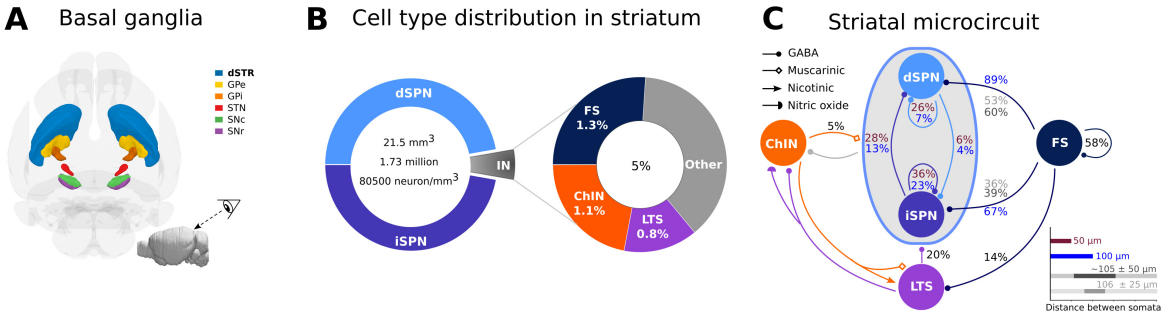
to input rates as well as correlations of the cortico-striatal input. To compensate for the loss of inputs we tested two strategies: 1. Strengthening of the remaining synaptic inputs, and 2. Rewiring by adding the lost glutamatergic synapses onto existing dendrites. Our results predict that at a single SPN level the effect of PD (i.e. the loss of dendrites and altered membrane properties) can be counteracted by either rewiring or strengthening the cortico-striatal inputs. Moreover, SPN dendritic atrophy and sprouting of FS axons significantly depletes the richness of the striatal network connectivity. Loss of higher order striatal motifs highlights the importance of morphological changes in addition to changes in electrophysiological properties. While the activity of the single neurons (SPNs) can be restored by adjusting the synaptic inputs, the intrastriatal structural changes would not be easily compensated for by simply increasing or decreasing the intrastriatal synaptic strengths. Our work thus highlights the importance of being able to investigate separately the role of the structural and electrophysiological changes occurring in neurodegenerative diseases such as Parkinson's disease. Here biophysically detailed *in-silico* reconstructions play an important role.

## RESULTS

PD progression is characterised by morphological changes of SPNs (dendritic atrophy) and FS (axonal growth) and changes in the neuron's membrane properties. To disentangle such changes, we first investigate how the morphological alterations reshape the striatal circuitry. Subsequently we study how the loss of cortico-striatal synapses may affect the response of individual SPNs and potential compensatory mechanisms.

### ***Changes of single neuron morphology in PD striatum***

We mimicked the gradual degeneration of the SPN (Fieblinger et al. (2014), Fieblinger et al. (2018), Alberquilla et al. (2020)) in PD by removing parts of the distal dendrites in three stages (PD1, PD2, PD3, see Methods). The control, non-PD stage, is denoted PD0. Examples of SPN PD morphologies, degenerated using the tool *treem* (Hjorth, Hellgren Kotaleski, and Kozlov (2021)), are illustrated in Figure 2 (A, dSPN, B iSPN, grey branches). Progressive degeneration of dendrites resulted in a reduction in the total dendritic length, number of branching points and number of primary dendrites (Figure 2C). Next, as reported in Gittis et al. (2011), we modelled the increase in the FS axonal length using *treem* (Figure 2D, red branches indicate axonal sprouting; Figure 2E, left panel; for details see Methods). The



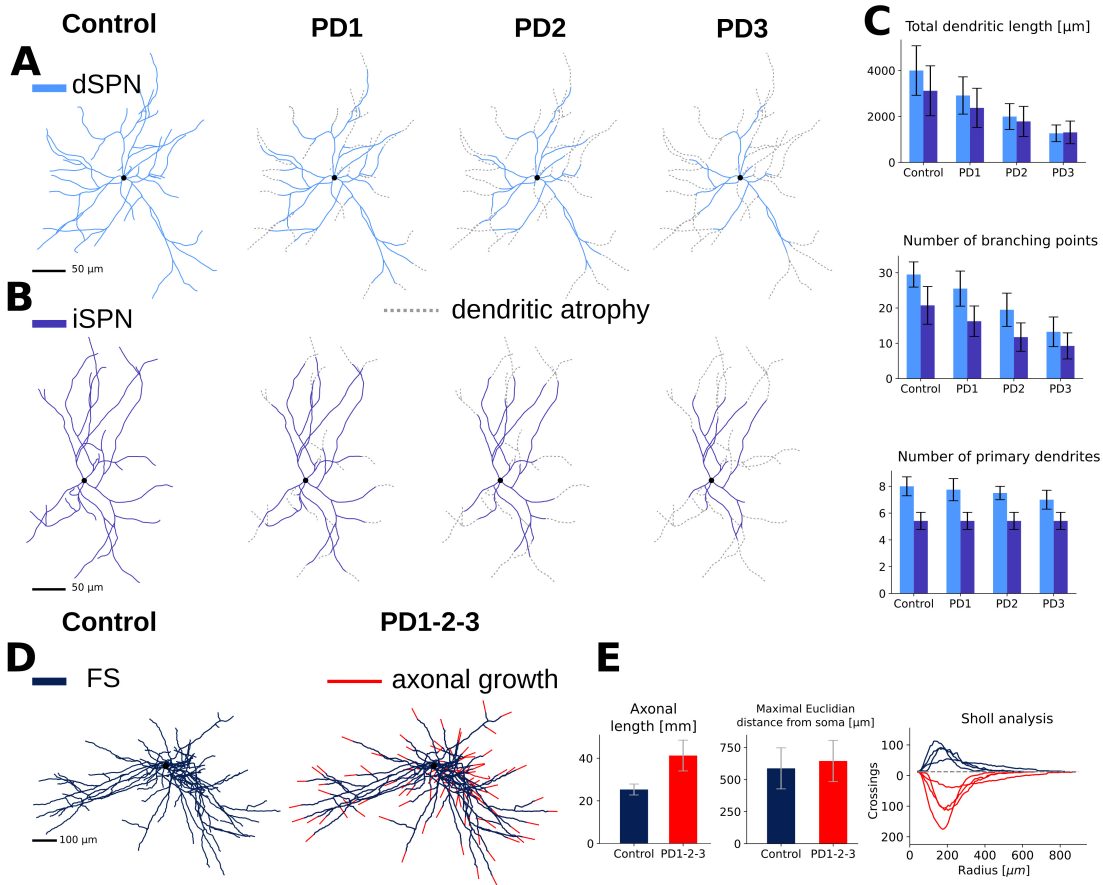
104 **Figure 1. Organization of the striatal microcircuit**

105 (A) View of the mouse basal ganglia nuclei (direction shown in the inset). The dorsal striatum (dSTR), globus pallidus external and internal segment (GPe and  
106 GPi, respectively), subthalamic nucleus (STN), substantia nigra pars reticulata and pars compacta (SNr and SNc, respectively) are shown in relative sizes. The  
107 colour coding is as indicated. The inset on the bottom right represents the entire mouse brain and the observer's view. (B) The mouse striatum is around 21.5  
108 mm<sup>3</sup> with a total of 1.73 million neurons which correspond to approximately 80 500 neurons/mm<sup>3</sup>. The main cells in the striatum are the striatal projection  
109 neurons (SPN), they constitute around 95% of the neurons and they are divided into two subpopulations (dSPN and iSPN). The remaining 5% of the neurons  
110 are interneurons. Fast-spiking (FS), cholinergic (ChIN) and low-threshold spiking (LTS) interneurons are included in this in-silico network. Together they  
111 account for around 3.2% of the neurons (around 64% of the interneuron types). (C) Connection probabilities between the neuronal subtypes included in the  
112 in-silico network were collected from published data. When more than one number refers to the same connection (arrow) they come from different publications.  
113 In particular the distance between the somatic pairs is different. Dark brown and blue refer to somatic pair distance within 50 μm and 100 μm, respectively;  
114 while dark and light grey refer to an average distance of about 105 ± 50 μm and 106 ± 25 μm, respectively.

115 average distance over which FS axons extended was not changed significantly in PD (Figure 2E, middle  
116 panel), but there was an increase in the number of grid crossings in the Sholl analysis (Figure 2E, right  
117 panel). In conclusion, the axonal trees of FS interneurons did not grow in a preferential direction but  
118 were denser than in control.

#### 141 **Predicting the network connectivity in the healthy and diseased state**

155 Dendritic atrophy of SPN results in loss of both SPN local connectivity as well as decreased  
156 cortico-striatal connectivity. On the other hand, FS axonal growth increases FS-iSPN connectivity and  
157 maintains almost invaried FS-dSPN connectivity. How these changes affect the striatal network structure  
158 beyond just a change in connection probabilities requires three dimensional reconstruction of the neuron  
159 morphologies and reconstruction of the network according to different states of PD. To this end, we used



127 **Figure 2. Morphological changes over Parkinson's disease (PD) stages in the model.**

128 The dendritic arborization of striatal projection neurons (dSPN and iSPN) is reduced in PD mice. Three different stages of the disease are simulated. PD1  
 129 refers to a mild starting phase, PD2 to a medium stage and PD3 to a very severe phase. Only soma and dendrites are shown for SPNs and the grey dotted  
 130 lines represent the dendritic branches that atrophied (A, B). Total dendritic length, number of branching points and number of primary dendrites for control  
 131 (healthy) and PD stages are represented as histograms (C). Axonal arborization of fast-spiking interneurons (FS) is increased in PD mice. Only soma and axon  
 132 are shown for FS and the red lines represent the axonal branches that have sprouted (D). The axonal length increased over 60% while the maximal euclidian  
 133 distance from soma (the radius of the smallest sphere containing the axon) does not change significantly. A significant increase in the number of grid crossings  
 134 by FS axons in PD is also reported (E).

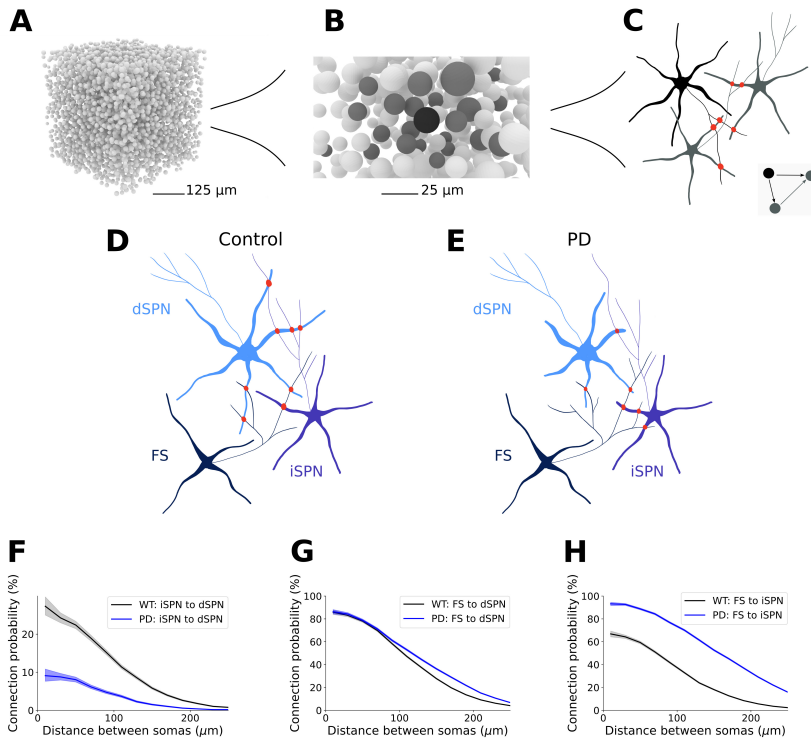
160 the modelling framework **Snudda**, presented in Hjorth et al. (2021, 2020). We first randomly placed  
 161 100 000 neurons with appropriate cell densities (approximately 80 500 neurons/mm<sup>3</sup>) and then putative  
 162 synapses between neuron pairs were detected based on proximity of their axons and dendrites. The initial  
 163 touch detection overestimates the connectivity, therefore the putative synapses were pruned in successive

164 steps (see Methods and Hjorth et al. (2021, 2020)) to match the experimental connection probability  
165 (Figure 1C). We refer to this as the healthy striatum or PD0. To avoid edge effects, when quantifying the  
166 local connectivity, only the very central neurons were considered for the analysis. In particular a subset  
167 of neurons closest to the centre of the cube are chosen and together with all their pre and postsynaptic  
168 neurons are selected (Figure 3 A, B, C; see Methods). We used the same strategy to generate the three  
169 stages of PD (see Methods). Because there is no cell loss, the distribution of the cells was retained (i.e.  
170 same as in PD0 network) but due to SPN dendritic atrophy and sprouting of FS axons, synaptic  
171 connectivity was different (Figure 3 D, E and Supplementary Figure 1). During PD, because of the  
172 morphological alteration, the connection probabilities between cell types decreased for all connections  
173 except FS-iSPN (Figure 3F, G, H; Supplementary Figure 2).

174 ***Topological characterization of the network in health and PD***

175 *Directed cliques in healthy and PD model of striatum* A change in the pairwise connection probability is  
176 not informative about how the full connectivity has been restructured due to the single-cell morphological  
177 changes (SPNs dendritic atrophy and FS axonal growth). To study the higher order properties of striatal  
178 networks we investigated the presence of specific motifs called directed cliques (Reimann et al. (2017)).  
179 A directed clique is a set of all-to-all connected neurons with a source and a sink. In this definition we are  
180 agnostic to the sign of the connection (excitatory or inhibitory). A directed clique constituted by  $n + 1$   
181 neurons is called a directed  $n$ -dimensional clique, or directed  $n$ -clique. For a rigorous definition of a  
182 directed  $n$ -clique see Method (Topological Measurements) and for examples or counterexamples of  
183 directed cliques see Figure 4 A1-4. These motifs are well suited to the study of the degeneration of  
184 striatal networks as in PD because they reveal complex patterns which were not visible from the analysis  
185 of single pairwise interactions.

186 We traced many directed cliques of dimension up to 13 in our model. In the healthy model  
187 6-dimensional cliques were the most abundant ( $10^7$ ) whereas 5-dimensional cliques were most numerous  
188 ( $10^5$ ) at stage PD2. In disease states (especially in PD2 and PD3) the number of directed cliques and their  
189 dimension drastically decreased (see Figure 4B) because of SPN dendritic atrophy. However cliques of  
190 dimension up to 13 are present in PD1 while the maximal clique dimension in PD0 is 12 (see Figure 4B).  
191 The mechanism underlying the formation of new higher dimensional cliques in PD1 is for example as  
192 follows: consider a 2-clique in PD0 consisting of two iSPNs and one dSPN. Now if, in PD1, a sprouted



142 **Figure 3. From morphologies to connectivity.**

143 Generating network connectivity using Snudda from reconstructed morphologies for healthy and PD networks. A) Example of positions of multi-compartmental  
144 neurons (somata) placed in a cube (5 000 somata are illustrated). A set of neurons in the centre of the cube, called kernel, is selected. All the pre- and post-  
145 synaptic neurons of the kernel form the core. The topological analysis is then performed on the kernel and core and only the cliques with at least one element  
146 in the kernel are kept to avoid edge effects. In B) only one neuron forms the kernel (in black) and the elements in the core are in dark grey. C) Illustration of  
147 touch detection between a neuron in the kernel and two of its partners in the core. The three neurons together form a clique (inset figure) and the synapses are  
148 shown in red. Illustration of connections between FS, dSPN and iSPN in the control network (D), and in PD (E). The loss of dendrites in PD causes a reduction  
149 in connectivity between the SPN neurons (here from 4 to 1), while the effect of FS axonal growth leads to new synapses on the iSPN (here from 1 to 3). F)  
150 The dendritic degeneration of the SPN leads to reduced pairwise connection probability at all soma-to-soma distances between SPN, here illustrated by the  
151 iSPN to dSPN connection probability. G) In accordance with data from Gittis et al. (2011) the growth of FS axons compensates for part of the degeneration of  
152 the dSPN morphologies, maintaining connection probability between the neuron types. H) For FS-iSPN connectivity the growth of the FS axons and locally  
153 increased synapse density compensates for the degeneration, leading to a doubling of the connectivity within 100 micrometres. Shaded regions in F, G and H  
154 represent the Wilson score interval.

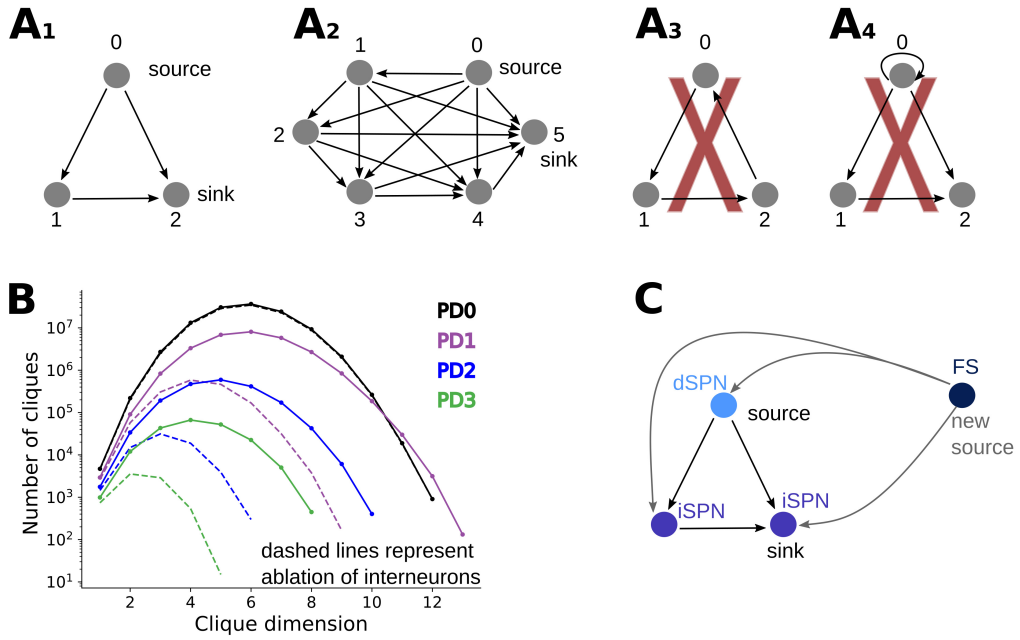
193 FS axon projects to all neurons in this clique it will create a 3-clique with FS as the source (schematized  
194 in Figure 4C). Just as in this example, because of their connection probability, FS are in the perfect

position to form cliques of higher dimensions (not containing ChIN). In particular FS are not postsynaptic to any other neuron type in the network (Figure 1C), so when they belong to a clique, one FS is always the source. In summary, SPN dendritic atrophy and FS axonal growth counter each other and only in PD1 condition we observed an increase in maximum clique dimension (while the total number of cliques in PD1 was lower than in PD0).

Interneurons, despite constituting only 5% of the striatal neuron population, have a key role in maintaining higher order network connectivity, especially during PD progression. To illustrate their role in directed clique formation we ablated all different types of interneurons (FS, LTS and ChIN) from the network. In the healthy network, ablation of interneurons did not drastically affect the count distribution of cliques (Figure 4B in log-scale, black solid and dotted line). However, removal of interneurons drastically reduced both the count as well as the maximum clique dimension in PD networks (Figure 4B dotted lines).

*Composition of directed cliques* To better understand which types of cliques are affected by PD progression we categorised cliques by their composition type as: all dSPN, all iSPN, at least one interneuron, dSPN and iSPN (for comparison between PD0 and PD2 see Figure 5 A; for comparison between all the PD stages in dimension 3 and 5 see Figure 5 B, C and Supplementary Figure 4 for cliques of other dimensions). Most directed cliques in the healthy network PD0 were exclusively formed by iSPNs and reached dimension 12 while in PD2 the majority of cliques contained at least one interneuron and reached dimension 10 (see Figure 5A). Without interneurons in PD2 the maximum clique dimension was only 6. These results show that during PD progression, cliques without interneurons were clearly more affected and decreased at a faster rate. In fact, cliques of dimension 5 either only containing dSPNs or dSPNs and iSPNs were absent in PD3 (Figure 5 C). From dimension 3, the cliques containing at least one interneuron are always the most abundant in PD (See supplementary Figure 4).

Directed cliques were further characterised by the number of synapses between all pairs of neurons composing the cliques (Figure 5 D, E). We found a threshold (30 for cliques in dimension 3 and 80 for cliques in dimension 5) such that cliques with a subthreshold number of synapses were more abundant in PD0, while cliques with a suprathreshold number of synapses, although generally fewer, were more present in PD2 (Figure 5 D, E: notice that below the threshold the black curve representing PD0 is above

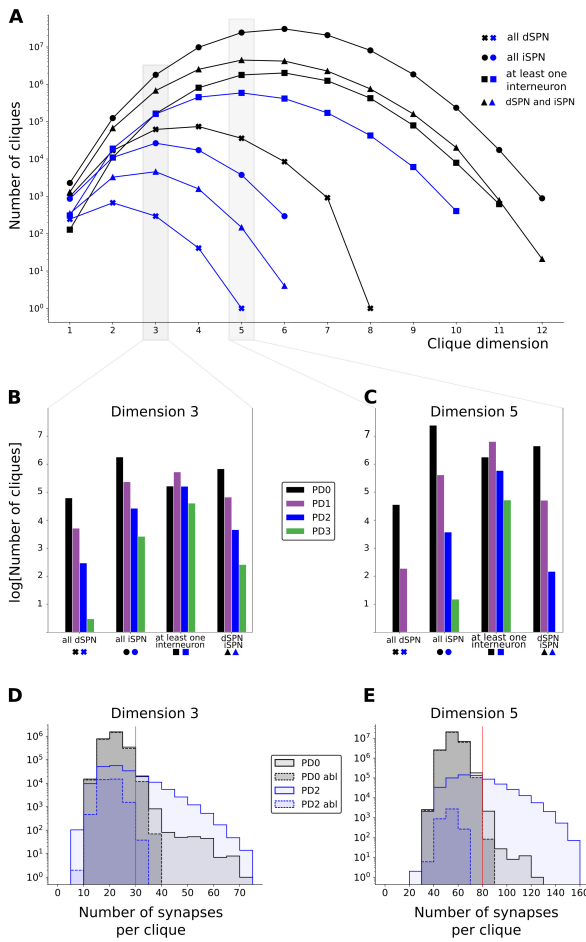


200 **Figure 4. Directed cliques and their presence in PD networks.**

201 (A) A directed clique is a set of all to all connected vertices, with a unique source and a unique sink (see: Methods: Topological measurements). A clique  
 202 composed of  $n+1$  vertices is called a  $n$ -clique. (A1) and (A2) are examples of a 2-clique and a 5-clique respectively. Figure (A3) represents instead a cyclic  
 203 structure in a directed graph, where a source and a sink are not present. This is therefore not an example of a directed clique. The graph represented in (A4)  
 204 is also not a directed clique, according to our definition, since we assume that directed graphs do not contain self loops. (B) Number of directed cliques in the  
 205 healthy network (PD0) and different Parkinsonian stages (PD1, PD2, PD3) as a function of the clique dimension in log-scale. Dashed lines represent directed  
 206 clique counts in networks where interneurons have been ablated (only direct striatal neurons (dSPNs) and indirect striatal neurons (iSPNs) are present in the  
 207 networks). (C) Schematic representation suggesting how during PD stages new high dimensional cliques can be formed. The axonal growth of fast-spiking  
 208 (FS) interneurons during PD progression can indeed determine connections from FS to existing directed cliques. The FS interneuron together with the neurons  
 209 composing the already existing directed clique then form a new directed clique with source FS. This mechanism explains why PD1 has higher dimensional  
 210 directed cliques than PD0, despite the dendritic atrophy of SPNs in the PD network.

223 the blue curve representing PD2 and above the threshold the opposite holds). Moreover in the ablated  
 224 networks the number of synapses per clique decreases faster in PD2 than in PD0 (Figure 5 D, E).

245 *The role of interneurons in network high connectivity* To confirm that interneurons are crucial for  
 246 maintaining the dimensionality of the cliques we progressively pruned the PD networks in two different



229 **Figure 5. Composition of directed cliques.**

230 The presence of directed cliques composed by only dSPN cells (x marker), only iSPN cells (circle marker), containing at least one interneuron (square marker),  
 231 containing both dSPN and iSPN (triangular marker) is analysed in figure A, B and C. Figure A: Number, in log scale, of directed cliques with specific neuron  
 232 compositions described above as a function of the clique dimension in the healthy network PD0 (blue curves) and at Parkinsonian stage PD2 (black curves).  
 233 Number, in log scale, of cliques in dimension 3 (B) and dimension 5 (C) in PD0 (in black), PD1 (in purple), PD2 (in blue) and PD3 (in green) subdivided within  
 234 the specific neuron compositions. D and E respectively represent the log scale histogram of cliques in dimension 3 and 5 with a given number of synapses, in  
 235 PD0 (light grey), PD0 ablated (dark grey dashed boundary), PD2 (light blue) and PD2 ablated (light blue dashed boundary). Vertical red lines represent the  
 236 thresholds such that cliques with a subthreshold number of synapses were more abundant in PD0, while cliques with a suprathreshold number of synapses were  
 237 more present in PD2.

247 ways and compared the results to that obtained in the corresponding ablated networks (network without  
 248 interneurons already represented in Figure 4B). First, we pruned synapses from the entire network

(including every cell type). Second, we only pruned SPN-SPN synapses (Figure 6 A, B, C and D, E, F, respectively). Because of the interneurons' involvement in high dimensional cliques, if their connectivity is kept fixed and only the SPN connectivity eroded (as in the second erosion) the maximal clique dimension is expected to be greater than the maximal of the ablated networks.

When starting from PD1, to mirror the directed clique count of the ablated (PD1) network, between 10-20% of the synapses had to be removed when eroding the entire network (Figure 6A) while between 30-40% of the connections had to be erased when removing only the SPN connectivity (Figure 6D). These percentages are expected to increase when considering more severe PD stages. In PD2 and PD3 around 30% and 40% network erosion respectively (Figure 6B-C) was needed to mimic the corresponding ablation. As expected, even when eroding only the SPN connectivity by 80% (PD2, Figure 6E) and 95% (PD3, Figure 6F), the maximal clique dimension obtained was one dimension greater than the corresponding maximal dimension in the ablated networks.

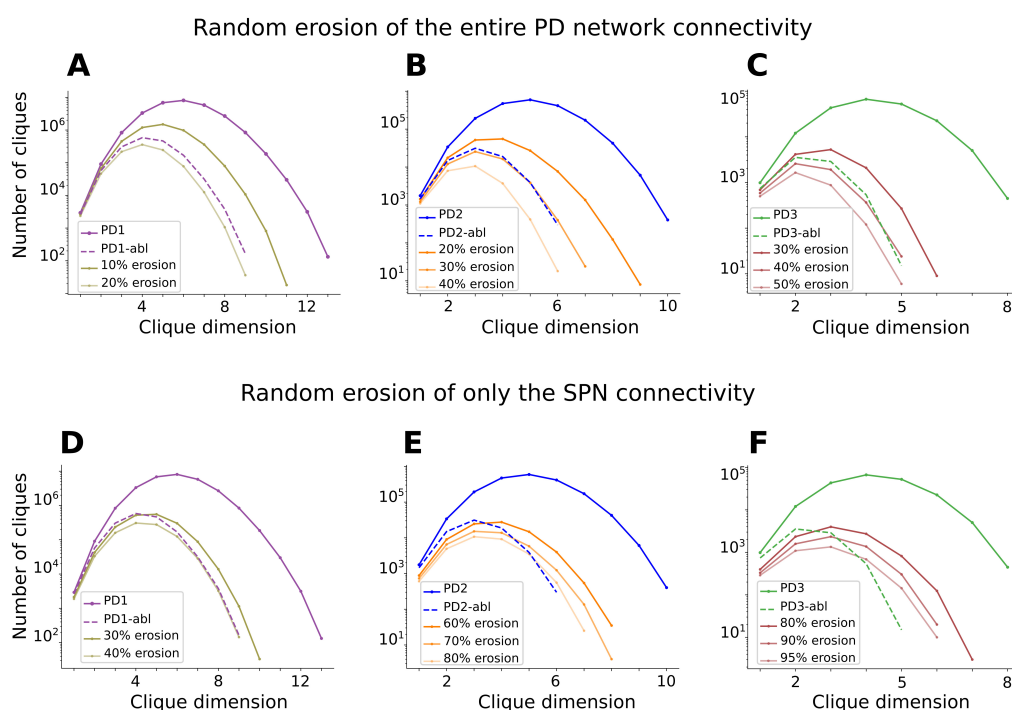
Independently on the erosion setting, it was possible to match the maximal number of cliques of the ablated networks with an eroded network. However, because of the discrepancy in the maximal clique dimensions, with clique dimensions dropping in the ablated networks, the shapes of the clique distributions of the eroded networks only match when all synapse types are eroded.

### *Transfer of cortical input to striatal output*

Another direct consequence of dendritic atrophy is loss of glutamatergic inputs. To investigate how this may affect the transfer of input from cortex (and thalamus), we simulated a set of Parkinsonian dSPN and iSPN and compared the neuron firing rate for different types of inputs with the healthy counterparts.

To this end, we used dSPN and iSPN which were tuned to reproduce physiological changes measured in Fiebinger et al. (2014) (see Methods). The dSPN electrophysiological models accounted for the increase in dSPN intrinsic excitability (Figure 7 top) while the iSPN models accounted for the decrease in iSPN intrinsic excitability (Figure 7 bottom).

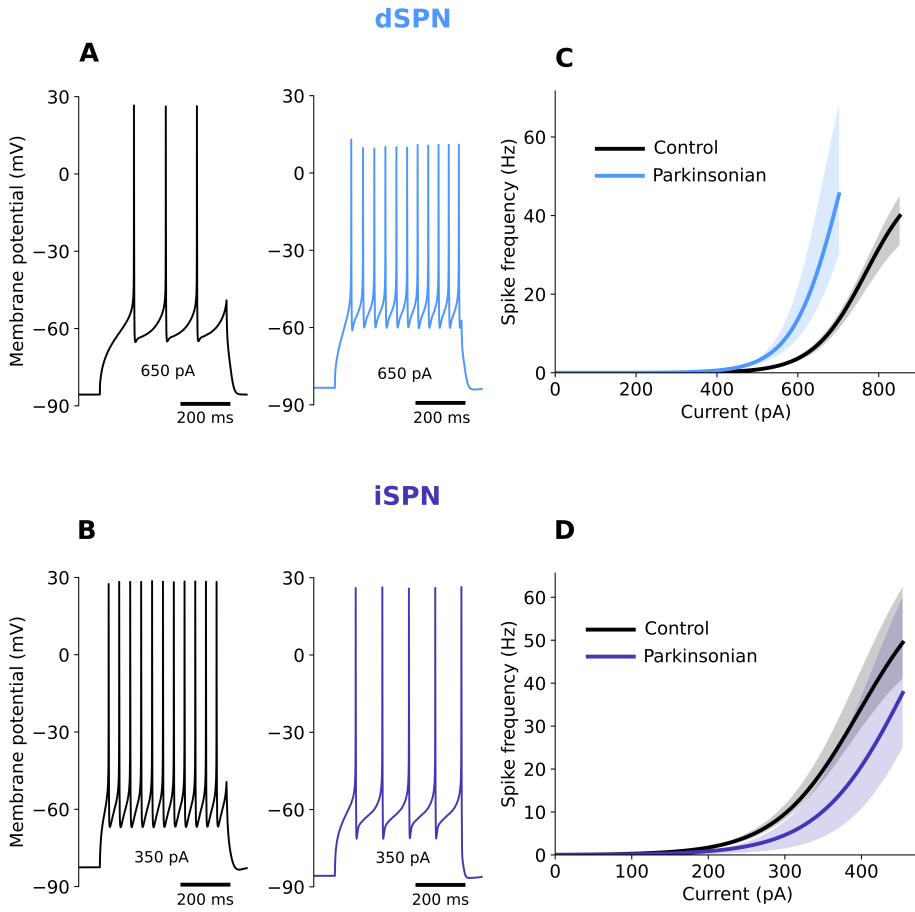
These models were then used to investigate the transfer of cortico-striatal inputs to the striatum. The number of cortico-striatal synapses (=size of the input ensemble) in the control case (PD0) was tuned for each morphology to obtain an output frequency of about 10 Hz when the synapses were receiving 5 Hz of Poisson type spiking input (see Methods and Supplementary Figure 4). For the PD2 condition we used *Snudda* to estimate the number of synapses remaining on the neurons after dendritic atrophy.



261 **Figure 6. Interneurons are key to maintaining network connectivity.**

262 Despite being only 5% of the neuron population, ablation of the interneurons leads to significant loss of connectivity in each PD stage. The importance of  
263 the interneurons can be observed by assessing how many random synapses (directed edges) in the network have to be removed to obtain a comparable effect  
264 to ablating the interneurons on directed clique counts. In PD1 (A), 10-20% of connections need to be eroded; in PD2 (B) around 30%, while in PD3 (C)  
265 approximately 40%. If instead only SPN synapses are removed, the fraction of synapses that need to be removed is even higher. In PD1 (B), 30-40% of the  
266 SPNs synapses need to be eroded, in PD2 (E) between 60-80% and PD3 (F) 80-95%.

290 The (remaining) synapses on the PD2 morphologies (Figure 8A, red circles) were not sufficient to  
291 equalise the output frequency obtained in healthy cells for the same input. Neurons in the PD2 stage  
292 spiked at a very low firing rate (Figure 8B-E compare grey and blue lines). Therefore, we used two  
293 strategies to compensate for the loss of synapses: the remaining synapses were strengthened by  
294 increasing their conductance (Figure 8A, middle panel) or the synapses on the atrophied dendrites were  
295 recovered and distributed over the remaining dendrites (synapses rewiring; Figure 8A, right panel). These  
296 two forms of compensations were done gradually to better quantify their effect (see Methods) and a  
297 schematization of the settings is illustrated in Figure 8A.



279 **Figure 7. Modelling of the electrophysiological properties of SPNs during PD.**

280 Changes of excitability and shape of the action potential in the striatal projection neurons' model of the direct pathway (dSPN, A) and indirect pathway  
281 (iSPN, B). Voltage traces and current-frequency response curves are shown for healthy neurons (Control, black lines) and neuron models adjusted to mimic  
282 physiological changes typical for PD (Parkinsonian, colour lines). Voltage plots illustrate discharge patterns of the healthy and PD cells in response to the  
283 same somatic direct current injection. Current-frequency curves are shown for the single-cell models, dSPN (C) and iSPN (D), using one morphology (up to 9  
284 variations) for each cell type and multiple fitted electrical parameter sets (up to 10 for each cell). Shaded regions represent range values.

298 With this setup we systematically varied the cortical input firing rate and pairwise correlation (60  
299 different input configurations) and measured the output firing rate of all the SPNs in their healthy state  
300 (PD0) and unhealthy states (PD2) with 10 types of compensations (see Methods for details). Either  
301 rewiring or strengthening of synapses was sufficient to match the output average firing rate of the PD2  
302 neurons with that of their healthy counterparts. Notably, given the difference in SPN excitability (Figure  
303 7), smaller compensation was needed for dSPNs as compared to the iSPNs (compare Figure 8C, E).

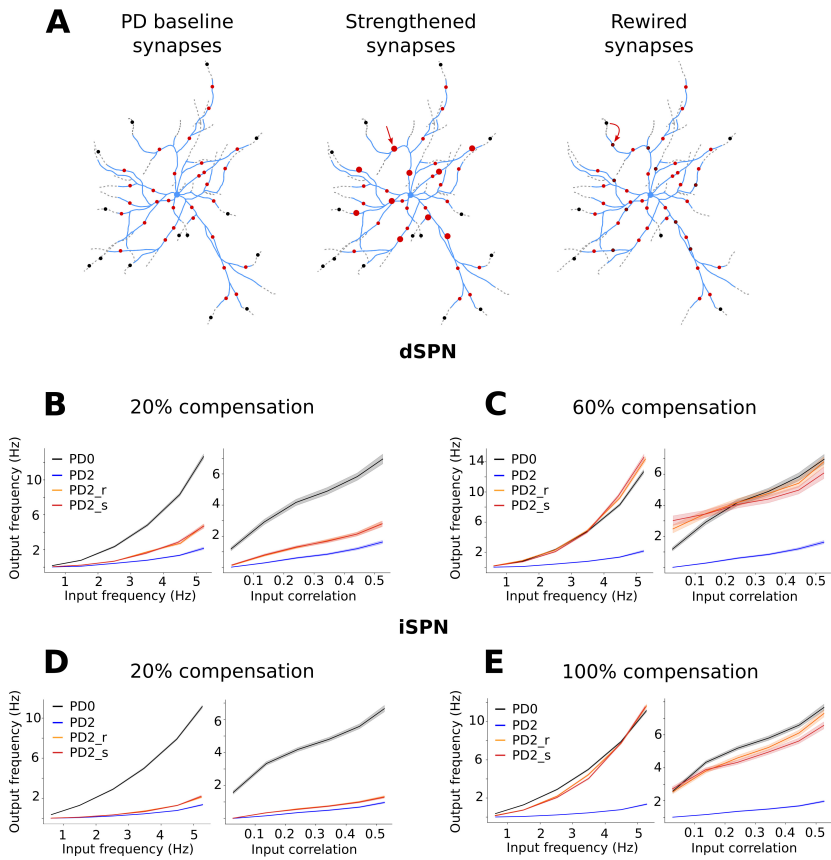
304 Typically, increase in correlations results in higher output firing rate. However, for dSPNs both rewiring  
305 and strengthening (when the compensation accounted for 60% or more) resulted in a reduction in the  
306 input firing rate (Supplementary Figure 5 and Supplementary Figure 7 for a conceptual explanation).

318 In summary, these results highlight that strengthening and rewiring (with and without correlations)  
319 have quite similar effects here, and that iSPN would need more compensation to approximate the output  
320 frequency obtained in the healthy case. However, here we have only focused on the feedforward transfer  
321 of cortical inputs to SPNs. Results may change if we consider both disease related changes in  
322 feedforward (due to FS axon sprouting) and recurrent inhibition (due to SPN dendrite atrophy).

## DISCUSSION

323 Parkinson's disease leads to several changes in the striatal neurons. In this in-silico study we used a  
324 biophysically detailed striatal microcircuit model. We investigated how the effects of PD on striatal  
325 neurons impact the richness of the striatal network connectivity and also predicted resulting changes  
326 occurring in the effective glutamatergic drive (in accordance to glutamatergic hyperactivity Campanelli,  
327 Natale, Marino, Ghiglieri, and Calabresi (2022)).

328 Progression of PD is accompanied by gradual changes in the neuron morphologies and intrastriatal  
329 synaptic connections. To understand how these changes affect the connectivity structure of the local  
330 striatal network we focused on directed cliques, a tool from computational topology. Here we observed  
331 that the number and dimension of directed cliques decreased as the disease progressed, highlighting the  
332 degeneration of higher order network connectivity structure. Unexpectedly, we also found that  
333 interneurons are crucial in both maintaining the network connectivity during PD and in the formation of  
334 high dimensional cliques (in particular due to sprouting of the FS axons). Most of high dimensional  
335 cliques in PD networks (dimension 3 or higher in PD1, dimension 2 or higher in PD2 and PD3 stages)  
336 contained at least one interneuron. Our clique count curves have shapes similar to those reported for the  
337 neocortical networks (Reimann et al. (2017) and Kanari et al. (2022)). However, there are notable  
338 quantitative differences between a striatal and a neocortical network in the number of cliques, maximal  
339 dimensions and behaviour of the curves when considering networks of degenerated neurons. These  
340 differences are likely to be due to the differences in the neuron types, pairwise connectivity, spatial  
341 distribution of neurons (e.g. layering in the neocortex) and strategies for modelling neuronal



307 **Figure 8. Striatal projection neurons (SPNs) responses to stimulation of cortico-striatal synapses in the control network (PD0) and during Parkinson-**

308 **son's disease (PD2).** (A) Because of the dendritic atrophy of SPNs (dotted grey branches), some cortico-striatal synapses are lost (black circles). The synapses

309 (red circles) on the remaining branches (light blue) are not sufficient to produce the same response as the healthy cells. For this reason two compensatory

310 mechanisms were implemented to restore the activity level. Percentages of the remaining synapses (20%, 40%, 60%, 80% and 100%) were strengthened

311 (larger circles in middle panel) or percentages of lost synapses were rewired (recovered and redistributed) on the remaining dendrites (dark red circles in right

312 panel). Different synaptic input frequencies (from 0.5 Hz to 5 Hz in steps of 0.5 Hz) and input correlations (from 0 to 0.5 in steps of 0.1) were used to

313 stimulate the neurons. Specifically all the combinations were considered and the output frequency is plotted either as function of the input frequency averaging

314 over the input correlations (left panels B, C, D, E) or as function of the input correlations averaging over the input frequencies (right panels B, C, D, E). Line

315 colours represent the output frequency of the healthy (PD0, black) neurons, the Parkinsonian ones (PD2, blue) as well as levels of rewiring (PD2\_r, orange) and

316 strengthening (PD2\_s, red). Specifically, (B) and (C) refer to dSPN when 20% and 60% compensation were applied respectively. (D) and (E) refer to iSPN

317 when 20% and 100% compensation were applied respectively.

342 degeneration. Our PD morphologies are directly degenerated (or grown) using treem, while other  
 343 methods such as used in Kanari et al. (2022) base their degeneration on topological descriptors of the

344 dendritic tree. Directed cliques indicate convergence of activity and therefore their presence in a network  
345 could imply emergence of synchrony in the network. Indeed, consistent with this, Reimann et al. (2017)  
346 related directed cliques in a neocortical microcircuit model to synchrony following stimulus from  
347 thalamus. However, the exact relationship between clique count and degree of correlations is not well  
348 understood. Moreover, in the striatum recurrent connections are GABAergic (inhibitory) and it is unclear  
349 whether directed cliques with inhibitory synapses have the same impact on network activity as the  
350 directed cliques with excitatory synapses. While a full simulation of striatal activity dynamics in different  
351 stages of PD is beyond the scope of the current initial work, our network can be used to investigate the  
352 effects of directed clique formation on striatal activity in future studies. In this scenario we can also  
353 investigate if the effect of the interneurons on the clique count in PD explains the importance of ChIN  
354 and LTS interneurons seen in PD (Shen, Zhai, and Surmeier (2022)).

355 Chronic dopamine depletion also induced many cell specific alterations in intrinsic excitability and  
356 glutamatergic synaptic connectivity. In healthy conditions a transient dopamine increase enhances the  
357 excitability of dSPN via D1 dopamine receptor signalling, while it decreases the excitability of iSPN  
358 through D2 dopamine receptor signalling (Surmeier, Graves, and Shen (2014)). Dopamine depletion in  
359 PD leads to increased intrinsic excitability in dSPNs (assessed via somatic current injection) and  
360 decreased excitability in iSPNs (Fieblinger et al. (2014), Ketzef et al. (2017)). Higher neuron excitability  
361 does not automatically imply higher firing rates in vivo, as network interactions, neuromodulation and  
362 various synaptic alterations can affect the final firing rate. How firing rates of dSPNs and iSPNs are  
363 altered in vivo during PD in response to ongoing cortical (and thalamic) activity is not clear from the  
364 literature. Conflicting results for dSPN and iSPN firing rates have been reported both in PD animal  
365 models and human patients (Singh et al. (2016), Beck, Singh, and Papa (2018), Valsky et al. (2020)).  
366 Several labs have reported that iSPNs have higher firing rate than dSPN in both anaesthetised and awake  
367 rats (Chen, Morales, Woodward, Hoffer, and Janak (2001), Mallet, Ballion, Le Moine, and Gonon  
368 (2006), Sharott et al. (2017)). Similarly, Parker et al. (2018) have reported higher  $\text{Ca}^{2+}$  event frequency  
369 in iSPNs compared to dSPNs during spontaneous activity in the mouse model of PD. However, Maltese,  
370 March, Bashaw, and Tritsch (2021) reported no significant difference between dSPN and iSPN  $\text{Ca}^{2+}$   
371 event frequency. Consistent with this, the spike firing rate of dSPNs and iSPNs in DA-depleted mice was  
372 comparable in both anaesthetised (Ketzef et al. (2017)) and awake (de la Torre-Martinez et al. (2023))  
373 states. Importantly for our study is that, to the best of our knowledge, no one has reported decreased

activity in any of the SPN neuron types, although the ensemble size of dSPNs might be decreased in vivo (in mice) (Maltese et al. (2021)). In our in-silico simulations of SPN glutamatergic activation we accounted for both the SPN morphological degenerations and intrinsic excitability changes. We found that Parkinsonian SPNs firing rates were much lower than their healthy counterparts while keeping the synaptic densities on the non-degenerated (remaining) dendritic branches and the individual synaptic strengths unchanged. This is a consequence of the majority of the spines being located on distal dendrites which account for the most part of the total dendritic length. To investigate how to restore the firing rate of SPNs to their healthy level, we tested two compensatory mechanisms: a) strengthening of the remaining synapses, and b) rewiring the lost synapses from the degenerated dendritic branches onto the surviving dendrites. For both these scenarios, we studied how the spike rate is influenced by several different combinations of input correlations and input frequencies. Interestingly, dSPNs and iSPNs needed different levels of compensation, in particular iSPNs needed more or stronger glutamatergic drive (60% and 100% recovery, respectively). Thus, our result predicts that the glutamatergic drive must undergo large quantitative changes to compensate for the effects of chronic dopamine depletion. This is in line with the glutamatergic hyperactivity (Campanelli et al. (2022)). Several experimental studies reported mechanisms that might contribute to a functionally more effective glutamatergic drive during dopamine depletion. While there is not much support for increased averaged spiking activity in cortex, rather the opposite (Underwood and Parr-Brownlie (2021), Viaro, Morari, and Franchi (2011), Bamford et al. (2004)), bursting develops and this might activate striatal neurons more effectively (Cagnan et al. (2019)). Furthermore, the parafascicular thalamic nucleus to iSPN drive is increased (Tanimura, Du, Kondapalli, Wokosin, and Surmeier (2019)), while at the same time, the intrastriatal lateral inhibition is decreased (López-Huerta et al. (2013), Taverna et al. (2008)). In addition, dopamine depletion itself might decrease presynaptic inhibition (Bamford et al. (2004)), it also leads to an increase in the striatal acetylcholine levels (Ztaou and Amalric (2019), Aosaki, Miura, Suzuki, Nishimura, and Masuda (2010), Ding et al. (2006)) (that might depolarise the SPNs via M1Rs in vivo), and alterations in the dynamics of the burst-pause response in ChINs (as this partly depends on D2R and D5R receptor activation). The latter might perhaps decrease presynaptic cortico-striatal inhibition (Aosaki et al. (2010), Pancani et al. (2014)). Moreover, the downregulation of glutamate transporters in striatal glia cells (Chung, Chen, Chan, and Yung (2008)), the enhancement of some NMDA subunit types in the membrane compartment (Gan, Qi, Mao, and Liu (2014)), and a change in the SPN A-type K<sup>+</sup> ion channel conductance and

404 dynamics could together produce larger summation of EPSPs in the SPN dendrites (Azdad et al. (2009)).  
405 Given our prediction of the significant amount of extra glutamatergic drive needed (60-100%) to at least  
406 allow the SPNs to fire as much as in the healthy state, it will be important to better quantify  
407 experimentally how these types of observed alterations contribute to the enhanced activation of striatal  
408 SPNs.

409 Using in-silico microcircuitry gives the advantage of making clear modelling assumptions and testing  
410 different scenarios to generate predictions as well as new questions. Moreover, using in-silico  
411 reconstructions allows us to disentangle the effect of the morphological and resulting network topological  
412 alterations from the more complex electrophysiological changes that the different neuron types undergo.  
413 Our Python code is open source with reproducible workflows that others can explore with modified  
414 assumptions.

415 We make predictions on how the clique count changes during PD, and although challenging, these  
416 could be measured experimentally. We also predict that chronic dopamine depletion in PD significantly  
417 increases the effective glutamatergic drive, especially to iSPNs. The glutamatergic hyperactivity is one  
418 significant driver of several of the morphological changes seen. Targeting some of the most contributing  
419 factors may be relevant for counteracting PD symptoms. For example, preventing or reversing  
420 glutamatergic hyperactivity might prevent alterations in the SPN morphology as well as the local network  
421 topology. We also think that the cellular level mechanisms involved in the benefits of PD add-on  
422 treatments such as transcranial magnetic stimulation (Nardone et al. (2020)) and rhythmic visual/auditory  
423 stimulation (De Icco et al. (2015), Koshimori and Thaut (2018)) needs to be better understood with  
424 regards to their therapeutic effects (Strafella, Paus, Barrett, and Dagher (2001), Raglio (2015), Koshimori  
425 and Thaut (2018), for example, are synaptic strengths altered or are the ensembles of co-activated  
426 cortico-striatal glutamatergic synapses changed. These treatments may use a mechanism of inducing  
427 effects similar to that of glutamatergic hyperactivity, but with reduced negative morphological  
428 consequences. One possibility is that these add-on treatments induce simultaneous dopamine and  
429 cortico-striatal glutamate release, wiring the two network pathways to fire together. Future experiments  
430 might shed light on which of the PD progression mechanisms has the largest impact and whether  
431 mechanism-specific treatments at certain stages of PD progression could prevent the mechanisms or  
432 mimic the mechanism without causing neuronal deterioration.

In summary, our work highlighted that just measuring the pairwise connectivity between neurons gives an incomplete description of the network connectivity. Here we did not assume neurons to connect in a completely random fashion, instead we used the neuron morphologies to further constrain the connectivity. We showed that directed cliques provided a richer characterization of the predicted changes in the network structure with respect to PD progression. We highlighted that the glutamatergic drive on SPN must undergo large quantitative changes to compensate for the effects of chronic dopamine depletion. Moreover the extent of these alterations should be different between dSPN and iSPN.

## MATERIALS AND METHODS

### *440 Network creation*

To investigate the striatal circuitry, 100 000 neurons were placed in a defined volume with appropriate cell densities (approximately 80 500 neurons/mm<sup>3</sup>) using the simulation environment Snudda, which allows to predict synaptic connectivity based on touch detection and a set of pruning rules (Hjorth et al. (2020), Hjorth et al. (2021)). Here the goal is to create both a healthy wild type (WT) network and a network representing the progression of Parkinson disease (PD).

### *446 Converting a healthy network into a Parkinsonian network*

*447 Change in neuron morphologies* During Parkinson's disease the striatal projection neurons' (SPN) dendrites degenerate, causing a reduction in the number of distal synapses. Fast-spiking (FS) axons, in turn, grow leading to an addition of GABAergic synapses. These two effects contribute to changing the connectivity of the network. Neurodegeneration was modelled as a progressive loss of the most distal fragments of the dendritic arbours of the SPN. This process resulted in systematic decrease of the total dendritic length while not much affecting the maximum radius of dendritic area and the number of primary dendrites similar to the data in Fieblinger et al. (2014). Morphological reconstructions were manipulated using Python module treem (Kozlov, A. K., 2021, Hjorth et al. (2021)). The initial WT morphologies were labelled PD0. Dendritic arbours were sampled at fixed spatial resolution 3 µm. SPN dendrites were shortened step-wise to mimic degeneration so that at each step of the algorithm one dendritic segment 3 µm long is truncated at every terminal. Morphologies after 10 and 20 truncation steps were labelled PD1 and PD2, respectively. The PD1 and PD2 neuron degenerations were based on mouse data from Fieblinger et al. (2014), while PD3 (30 steps) corresponds to a greater dendritic loss mimicking

what the human cells exhibit. Mean total dendritic length in our model is 3997.9  $\mu\text{m}$  (100%), 2890.8  $\mu\text{m}$  (72%), 1984.6  $\mu\text{m}$  (50%) and 1288.6  $\mu\text{m}$  (32%) for dSPN at PD0, PD1, PD2 and PD3, respectively; 3116.7  $\mu\text{m}$  (100%), 2362.5  $\mu\text{m}$  (76%), 1774.5  $\mu\text{m}$  (57%) and 1302  $\mu\text{m}$  (42%) for iSPN at PD0, PD1, PD2 and PD3, respectively (Figure 2A-C). To mimic the rapid growth of FS axons, we extended each axonal terminal of PD0 FS morphologies by 61  $\mu\text{m}$  and kept them unchanged between pathological PD stages 1-3. This resulted in the mean total axonal length 25572  $\mu\text{m}$  (100%) and 41249  $\mu\text{m}$  (161.3% cf. 161.8% in Gittis et al. (2011)) for FS at PD0 and PD1-2-3, respectively (Figure 2D-E).

*Evolution of striatal network structure in PD* There are different ways to generate the PD network. One approach is to start from the complete WT network, and remove the synapses that were placed on dendritic branches lost during the degeneration of the morphologies (degeneration method). This was done by swapping the WT morphologies for their corresponding PD morphologies, keeping the location and orientation and identifying which synapses are no longer attached to a dendrite. Another approach is to start with the PD morphologies in the corresponding locations and perform a new touch detection to determine where the synapses are (de novo method). In the first case the degenerated synapses were in the same location as before, but the extra FS synapses were missing. In the second case, the extra FS synapses were included, but the remaining synapses were not in the same location as before. To compensate for this, a hybrid method was implemented, where the synapses from the degeneration method and the de novo method were combined. In addition, there was also a difference in the number of synapses detected between the two methods, since in the first case pruning was done before degeneration, and in the second case degeneration was done before pruning, (see Supplementary Figure 1). In the hybrid method the number of synapses between neuron types was tuned to match those detected in the de novo method. The fraction of synapses remapped, i.e. synapses taken from the de novo method and added to the degenerated method's set of synapses, is called the remapping fraction. In summary, the hybrid method retained the position for the remaining synapses, while adding the new FS synapses to the network. It also retained a comparable number of synapses as a de novo detected PD network.

#### Topological measurements

Directed cliques can be used to measure higher order connectivity patterns in directed graphs. Following Reimann et al. (2017) a directed graph is defined as a pair of sets  $(V, E)$  equipped with an injective

488 function  $\tau : E \rightarrow V \times V$  where  $V$  is the set of vertices,  $E$  is the set of directed edges and assigns to a  
489 directed edge its source and target respectively. Furthermore it is assumed that a directed graph has no  
490 self loops (i.e. if  $\tau(e) = (v_1, v_2)$  then  $v_1 \neq v_2$ ). If  $\tau(e) = (v_1, v_2)$ , we call  $e$  a directed edge from  $v_1$  to  $v_2$ .  
491 Notice that the injectivity assumption implies that it is not possible to have more than one directed edge  
492 from  $v_1$  to  $v_2$ . Two vertices  $v_1$  and  $v_2$  can however be reciprocally connected with one directed edge from  
493  $v_1$  to  $v_2$  and one directed edge from  $v_2$  to  $v_1$ . Two vertices  $v_1$  and  $v_2$  in a directed graph are said to be  
494 connected if there is either an edge from  $v_1$  to  $v_2$ , or an edge from  $v_2$  to  $v_1$ , or both. A vertex  $v$  of a  
495 directed graph is called a *source* if it can only be the source of one or more directed edges, i.e.  $v$  can only  
496 appear in the first coordinate of the image of the function . In the opposite way, a vertex  $w$  is a *sink* if it  
497 can only be the target of one or more directed edges, i.e.  $w$  can only appear in the second coordinate of  
498 the image of the function . Informally one can say that all the edges containing a source are from this  
499 vertex and all the edges containing a sink are to this vertex. A directed clique is a set of vertices in a  
500 directed graph which are all to all connected and there exists a unique source and a unique sink among  
501 them. A directed clique consisting of  $n + 1$  vertices is called a clique of dimension  $n$  or directed  
502  $n$ -clique. If a partial order is defined on the vertices of a directed graph, where  $v_1 < v_2$  if there is an edge  
503 from  $v_1$  to  $v_2$ , a directed clique is a totally ordered subset of the vertices whose smallest element is the  
504 source and the largest element the sink. Directed cliques can be thought of as feedforward motifs from  
505 the source to the sink (See Figure 4 A1-4). In this article a directed graph is a structural network of  
506 neurons where vertices represent neurons and a directed edge represents the presence of synapses  
507 connecting a presynaptic neuron to a postsynaptic neuron. The source of a directed clique can then be  
508 seen as a neuron which is presynaptic to all the other neurons in the clique while the sink is a neuron  
509 which is postsynaptic to all the other neurons in the clique.

510 ***Selection of the core of the network***

511 It is important for the analysis that the neurons investigated have all their connected pre- and  
512 post-synaptic partners included in the network. To avoid potential edge effects a set of neurons (referred  
513 to as *kernel* neurons here) at the centre of the network is selected. All the neurons (both pre- and  
514 post-synaptic) connected to the kernel neurons were identified and labelled as the *core* together with the  
515 kernel neurons. Without this the connectivity for the neurons included in the analysis would be  
516 underestimated. Directed clique analysis was performed for neurons in the core and all cliques were

517 required to have at least one neuron belonging to the set of kernel neurons. All the results shown were  
518 obtained using a kernel of 8 neurons, 4 dSPNs and 4 iSPNs which resulted in a core of 2712 neurons (out  
519 of 100 000). The maximal distance between neurons in the kernel and their connected pre-or-postsynaptic  
520 neurons was around 550 µm. Also cores formed from kernels with exclusively dSPNs or iSPNs have  
521 been analysed, but because SPNs are intermixed within the striatum and present in equal number, a  
522 mixed kernel was preferred.

523 ***Simulation of cortical input to dSPN and iSPN neurons***

524 *Models of striatal projection neurons* Computational models of the healthy dSPN and iSPN cells were  
525 taken from the previous studies (Hjorth et al. (2020), Hjorth et al. (2021)). We refer the reader to them for  
526 details of the equations describing the time evolution of the membrane voltage. Several neuron models of  
527 each type (n=4) were fitted to experimental data (Hjorth et al. (2020), Figure 2 and Figure S3). Every  
528 model was characterised by a unique dendritic morphology, rheobase current and a current-frequency  
529 relation. Evolutionary parameter fitting algorithm (Van Geit et al. (2016)) provides multiple electrical  
530 parameter sets (up to 10) for each neuron model. To introduce more physiological variability within the  
531 neuron populations, the optimised parameter sets were combined with modified dendritic morphologies  
532 (9 variations of each reconstruction using scaling factors from 0.6 to 1.4 and random rotations of the  
533 dendritic branches at the branching points). All morpho-electric combinations were then simulated and  
534 validated against physiological features of the experimental populations as in Hjorth et al. (2020).

535 *Change in SPNs electrophysiology* Stage PD2 of the cell morphology modification was used to model the  
536 mouse PD network throughout. Electric parameters of the model SPN cells were manually adjusted to  
537 reproduce physiological changes observed experimentally in 6-OHDA lesioned mice (Fieblinger et al.  
538 (2014)). In dSPN models, both the fast sodium current and the transient potassium currents were reduced  
539 to account for the decrease in the action potential amplitude and afterhyperpolarization (AHP), the  
540 increase in excitability was mainly explained by the shorter total dendritic length (leading to higher input  
541 resistance of the neuron). Reduced excitability of iSPN cells in PD was achieved through strengthening  
542 of the inward rectifying potassium current and a corresponding increase of the leak conductance to  
543 maintain the unchanged resting membrane potential. Transient potassium current was also increased in

544 PD iSPN's to match the stronger AHP. Voltage traces and current-frequency responses of the healthy and  
545 PD SPN models are shown in Figure 7.

546 ***Setting and stimulating the input and compensatory mechanisms***

547 Both healthy and Parkinsonian SPNs were simulated using cortico-striatal drive to investigate the change  
548 in their output frequency. The number of input spike trains ( $n$ ) received by a neuron was determined by  
549 the neuron morphology and the type of compensation (see below). The number of synapses which were  
550 distributed on the PD0 morphologies was tuned to achieve an average output frequency of 10 Hz when  
551 the synapses were receiving 5 Hz of Poisson spike train without correlation. Using Snudda an estimate of  
552 the remaining synapses on the PD2 morphologies was obtained (47.5% and 53.25% for dSPN and iSPN  
553 respectively). Because of the reduction in the dendritic length and number of synapses (compared to  
554 PD0) the output frequencies of these neurons were lower than in the healthy counterparts. Hence, two  
555 compensatory strategies were implemented to restore the activity level. Strengthening the (remaining)  
556 synapses by 20%, 40%, 60%, 80% and 100% and rewiring the lost synapses (which were located on the  
557 branches that atrophied) by the same percentages. The base synaptic conductance is 0.5 nS and during  
558 the strengthening first the difference between the total synaptic conductance in PD0 and PD2 was  
559 calculated (number of missing synapses times 0.5 nS), then a percentage of this value divided by the  
560 number of synapses in PD2 was added to the base conductance of the latter. Hence in the 100%  
561 strengthening compensation step despite the number of synapses being different the total synaptic  
562 conductance is the same. Analogously, a percentage of the missing synapses was added at each step so  
563 that in the final case the number of synapses in PD2 was the same as PD0. Each input spike train was  
564 connected to the SPN with an excitatory synapse. Synapses were modelled as in Hjorth et al. (2020).  
565 Synapses were activated using Poisson spike trains of average rate  $\lambda$  and pairwise correlation  $c$ . The  
566 pairwise correlation,  $c$ , of each input stream is generated by first creating a mother Poisson spike train of  
567 frequency,  $f$ , and  $n$  child Poisson spike trains of frequency  $(1 - p) \cdot f$ . Where  $p = c$  is the probability that  
568 a mother spike is transferred to the child spike train. We systematically varied both  $\lambda$  [= 0.5 : 0.1 : 5 Hz]  
569 and  $c$  [= 0 : 0.1 : 0.5]. This resulted in 60 different combinations of input rate and correlations. All the  
570 60 combinations between frequency and correlation were simulated for each stage (healthy, Parkinsonian,  
571 and 10 different compensations), for a total of 720 sets of simulations (per cell type). Each set consisted  
572 of several combinations of morphologies and electric parameters, and for each combination 10

573 simulations, which differed in the synapse distribution, were performed. The corresponding results are  
574 illustrated using heatmaps in Supplementary Figure 5 and 6 for dSPN and iSPN respectively. A single  
575 square in the heatmap represents the average over one set of simulations (which includes the different  
576 combinations of morphologies, parameters and synapse distributions). In summary, all the scenarios  
577 (PD0, PD2 and PD2 compensated) were simulated using all the possible combinations between  
578 frequency and correlation. For each pair (frequency, correlation) the stimulation lasted 10 seconds and a  
579 2 second recovery period was included between pairs. In total 720 sets of simulations were reproduced  
580 (12 main scenarios including PD0, PD2, 5 strengthening and 5 rewiring times 10 different input  
581 frequencies times 6 different input correlations) for each combination of morphology and electric  
582 parameter. Each of this was repeated 10 times to include variability in the synaptic distributions.

583 ***Simulation and data analysis tools***

584 We used treem, a Python module (Kozlov (2021), <https://github.com/aleko/treem>), to modify the  
585 morphology to account for the changes that occur in PD. We used Snudda, the modelling framework  
586 written in Python (<https://github.com/Hjorthmedh/Snudda>) to create the networks (placement, touch  
587 detection and pruning) and setup the inputs. Neuron simulations were then performed using NEURON  
588 via Snudda. The number of directed cliques was computed using the software Flagser-count  
589 (<https://github.com/JasonPSmith/flagser-count>), an adaptation of Flagser  
590 (<https://github.com/luetge/flagser>) which deals with the more general problem of computing the  
591 homology and persistent homology of directed graphs. As a Python API for Flagser we refer to pyflagser  
592 (<https://github.com/giotto-ai/pyflagser>). The computations were enabled by resources provided by the  
593 National Academic Infrastructure for Supercomputing in Sweden (NAIIS) at PDC KTH partially funded  
594 by the Swedish Research Council through grant agreement no. 2022-06725.

## ACKNOWLEDGMENTS

595 We thank: PhD Jason Smith for all the support regarding flagser-count; Tor Kjellsson Lindblom for the  
596 help setting up the simulations on Dardel; William Scott Thompson for the precious Blender advice; PhD  
597 Johanna Frost Nylén and PhD Yvonne Johansson for all the insightful conversations; and PhD Barbara  
598 Mahler for her support. Finally we thank Prof. Gilad Silberberg and Prof. Sten Grillner for the  
599 enlightening discussions.

Authors: I. Carannante, M. Scolamiero, J.J.J. Hjorth, A. Kozlov, B. Bekkouche, L. Guo, A. Kumar, W. Chacholski and J. Hellgren Kortaleski

600 The computations were enabled by resources provided by the National Academic Infrastructure for  
601 Supercomputing in Sweden (NAIIS) at PDC KTH partially funded by the Swedish Research Council  
602 through grant agreement no. 2022-06725.

## SUPPORTING INFORMATION

603 [pdf of Supplementary Material provided]

## COMPETING INTERESTS

604 The authors declare that the research was conducted in the absence of any commercial or financial  
605 relationships that could be construed as a potential conflict of interest.

606

## REFERENCES

608

- 609 Alberquilla, S., Gonzalez-Granillo, A., Martín, E. D., & Moratalla, R. (2020). Dopamine regulates spine density in striatal  
610 projection neurons in a concentration-dependent manner. *Neurobiology of disease*, 134, 104666.
- 611 Aosaki, T., Miura, M., Suzuki, T., Nishimura, K., & Masuda, M. (2010). Acetylcholine–dopamine balance hypothesis in the  
612 striatum: An update. *Geriatrics & gerontology international*, 10, S148–S157.
- 613 Azdad, K., Chàvez, M., Bischoff, P. D., Wetzel, P., Marescau, B., De Deyn, P. P., ... Schiffmann, S. N. (2009).  
614 Homeostatic plasticity of striatal neurons intrinsic excitability following dopamine depletion. *PloS one*, 4(9), e6908.
- 615 Bamford, N. S., Zhang, H., Schmitz, Y., Wu, N.-P., Cepeda, C., Levine, M. S., ... Sulzer, D. (2004). Heterosynaptic  
616 dopamine neurotransmission selects sets of corticostriatal terminals. *Neuron*, 42(4), 653–663.
- 617 Beck, G., Singh, A., & Papa, S. M. (2018). Dysregulation of striatal projection neurons in parkinson's disease. *Journal of*  
618 *Neural Transmission*, 125, 449–460.
- 619 Bergman, H., Wichmann, T., Karmon, B., & DeLong, M. (1994). The primate subthalamic nucleus. ii. neuronal activity in  
620 the mptp model of parkinsonism. *Journal of neurophysiology*, 72(2), 507–520.
- 621 Cagnan, H., Mallet, N., Moll, C. K., Gulberti, A., Holt, A. B., Westphal, M., ... others (2019). Temporal evolution of beta

Authors: I. Carannante, M. Scolamiero, J.J.J. Hjorth, A. Kozlov, B. Bekkouche, L. Guo, A. Kumar, W. Chacholski and J. Hellgren Kortaleski

- 622 bursts in the parkinsonian cortical and basal ganglia network. *Proceedings of the National Academy of Sciences*, 116(32),  
623 16095–16104.
- 624 Campanelli, F., Natale, G., Marino, G., Ghiglieri, V., & Calabresi, P. (2022). Striatal glutamatergic hyperactivity in  
625 parkinson's disease. *Neurobiology of Disease*, 168, 105697.
- 626 Chen, M.-T., Morales, M., Woodward, D. J., Hoffer, B. J., & Janak, P. H. (2001). In vivo extracellular recording of striatal  
627 neurons in the awake rat following unilateral 6-hydroxydopamine lesions. *Experimental neurology*, 171(1), 72–83.
- 628 Chung, E., Chen, L., Chan, Y., & Yung, K. (2008). Downregulation of glial glutamate transporters after dopamine  
629 denervation in the striatum of 6-hydroxydopamine-lesioned rats. *Journal of Comparative Neurology*, 511(4), 421–437.
- 630 De Icco, R., Tassorelli, C., Berra, E., Bolla, M., Pacchetti, C., & Sandrini, G. (2015). Acute and chronic effect of acoustic  
631 and visual cues on gait training in parkinson's disease: a randomized, controlled study. *Parkinson's Disease*, 2015.
- 632 de la Torre-Martinez, R., Ketzef, M., & Silberberg, G. (2023). Ongoing movement controls sensory integration in the  
633 dorsolateral striatum. *Nature Communications*, 14(1), 1004.
- 634 Ding, J., Guzman, J. N., Tkatch, T., Chen, S., Goldberg, J. A., Ebert, P. J., ... Surmeier, D. J. (2006). Rgs4-dependent  
635 attenuation of m4 autoreceptor function in striatal cholinergic interneurons following dopamine depletion. *Nature  
636 neuroscience*, 9(6), 832–842.
- 637 Doya, K. (2008). Modulators of decision making. *Nature neuroscience*, 11(4), 410–416.
- 638 Fieblinger, T., Graves, S. M., Sebel, L. E., Alcacer, C., Plotkin, J. L., Gertler, T. S., ... others (2014). Cell type-specific  
639 plasticity of striatal projection neurons in parkinsonism and l-dopa-induced dyskinesia. *Nature communications*, 5(1),  
640 5316.
- 641 Fieblinger, T., Zanetti, L., Sebastianutto, I., Breger, L., Quintino, L., Lockowandt, M., ... Cenci, M. (2018). Striatonigral  
642 neurons divide into two distinct morphological-physiological phenotypes after chronic l-dopa treatment in parkinsonian  
643 rats. *Scientific reports*, 8(1), 10068.
- 644 Filipović, M., Ketzef, M., Reig, R., Aertsen, A., Silberberg, G., & Kumar, A. (2019). Direct pathway neurons in mouse  
645 dorsolateral striatum in vivo receive stronger synaptic input than indirect pathway neurons. *Journal of neurophysiology*,  
646 122(6), 2294–2303.

Authors: I. Carannante, M. Scolamiero, J.J.J. Hjorth, A. Kozlov, B. Bekkouche, L. Guo, A. Kumar, W. Chacholski and J. Hellgren Kotaleski

- 647 Gan, J., Qi, C., Mao, L.-M., & Liu, Z. (2014). Changes in surface expression of n-methyl-d-aspartate receptors in the  
648 striatum in a rat model of parkinson's disease. *Drug design, development and therapy*, 165–173.
- 649 Gittis, A. H., Hang, G. B., LaDow, E. S., Shoenfeld, L. R., Atallah, B. V., Finkbeiner, S., & Kreitzer, A. C. (2011). Rapid  
650 target-specific remodeling of fast-spiking inhibitory circuits after loss of dopamine. *Neuron*, 71(5), 858–868.
- 651 Hjorth, J. J., Hellgren Kotaleski, J., & Kozlov, A. (2021). Predicting synaptic connectivity for large-scale microcircuit  
652 simulations using snudda. *Neuroinformatics*, 19(4), 685–701.
- 653 Hjorth, J. J., Kozlov, A., Carannante, I., Frost Nylén, J., Lindroos, R., Johansson, Y., ... others (2020). The microcircuits of  
654 striatum in silico. *Proceedings of the National Academy of Sciences*, 117(17), 9554–9565.
- 655 Kanari, L., Dictus, H., Chalimourda, A., Arnaudon, A., Van Geit, W., Coste, B., ... Markram, H. (2022). Computational  
656 synthesis of cortical dendritic morphologies. *Cell Reports*, 39(1).
- 657 Ketzef, M., Spigolon, G., Johansson, Y., Bonito-Oliva, A., Fisone, G., & Silberberg, G. (2017). Dopamine depletion impairs  
658 bilateral sensory processing in the striatum in a pathway-dependent manner. *Neuron*, 94(4), 855–865.
- 659 Koshimori, Y., & Thaut, M. H. (2018). Future perspectives on neural mechanisms underlying rhythm and music based  
660 neurorehabilitation in parkinson's disease. *Ageing research reviews*, 47, 133–139.
- 661 Kozlov, A. K. (2021). *treem - neuron morphology processing tool*. Zenodo. Retrieved from  
662 <https://doi.org/10.5281/zenodo.4890844> doi: 10.5281/zenodo.4890844
- 663 López-Huerta, V. G., Carrillo-Reid, L., Galarraga, E., Tapia, D., Fiordelisio, T., Drucker-Colin, R., & Bargas, J. (2013). The  
664 balance of striatal feedback transmission is disrupted in a model of parkinsonism. *Journal of Neuroscience*, 33(11),  
665 4964–4975.
- 666 Mallet, N., Ballion, B., Le Moine, C., & Gonon, F. (2006). Cortical inputs and gaba interneurons imbalance projection  
667 neurons in the striatum of parkinsonian rats. *Journal of Neuroscience*, 26(14), 3875–3884.
- 668 Mallet, N., Pogosyan, A., Márton, L. F., Bolam, J. P., Brown, P., & Magill, P. J. (2008). Parkinsonian beta oscillations in the  
669 external globus pallidus and their relationship with subthalamic nucleus activity. *Journal of neuroscience*, 28(52),  
670 14245–14258.

- 671 Maltese, M., March, J. R., Bashaw, A. G., & Tritsch, N. X. (2021). Dopamine differentially modulates the size of projection  
672 neuron ensembles in the intact and dopamine-depleted striatum. *Elife*, 10, e68041.
- 673 Markram, H., Muller, E., Ramaswamy, S., Reimann, M. W., Abdellah, M., Sanchez, C. A., . . . Schürmann, F. (2015).  
674 Reconstruction and simulation of neocortical microcircuitry. *Cell*, 163(2), 456–492.
- 675 McNeill, T. H., Brown, S. A., Rafols, J. A., & Shoulson, I. (1988). Atrophy of medium spiny i striatal dendrites in advanced  
676 parkinson's disease. *Brain research*, 455(1), 148–152.
- 677 Nardone, R., Versace, V., Brigo, F., Golaszewski, S., Carnicelli, L., Saltuari, L., . . . Sebastianelli, L. (2020). Transcranial  
678 magnetic stimulation and gait disturbances in parkinson's disease: a systematic review. *Neurophysiologie Clinique*, 50(3),  
679 213–225.
- 680 Pancani, T., Bolarinwa, C., Smith, Y., Lindsley, C. W., Conn, P. J., & Xiang, Z. (2014). M4 machr-mediated modulation of  
681 glutamatergic transmission at corticostriatal synapses. *ACS chemical neuroscience*, 5(4), 318–324.
- 682 Parker, J. G., Marshall, J. D., Ahanonu, B., Wu, Y.-W., Kim, T. H., Grewe, B. F., . . . others (2018). Diametric neural  
683 ensemble dynamics in parkinsonian and dyskinetic states. *Nature*, 557(7704), 177–182.
- 684 Raglio, A. (2015). Music therapy interventions in parkinson's disease: the state-of-the-art. *Frontiers in neurology*, 6, 185.
- 685 Raz, A., Vaadia, E., & Bergman, H. (2000). Firing patterns and correlations of spontaneous discharge of pallidal neurons in  
686 the normal and the tremulous 1-methyl-4-phenyl-1, 2, 3, 6-tetrahydropyridine vervet model of parkinsonism. *Journal of  
687 Neuroscience*, 20(22), 8559–8571.
- 688 Redgrave, P., Prescott, T. J., & Gurney, K. (1999). The basal ganglia: a vertebrate solution to the selection problem?  
689 *Neuroscience*, 89(4), 1009–1023.
- 690 Reimann, M. W., Nolte, M., Scolamiero, M., Turner, K., Perin, R., Chindemi, G., . . . Markram, H. (2017). Cliques of  
691 neurons bound into cavities provide a missing link between structure and function. *Frontiers in computational  
692 neuroscience*, 11, 48.
- 693 Sharott, A., Vinciati, F., Nakamura, K. C., & Magill, P. J. (2017). A population of indirect pathway striatal projection  
694 neurons is selectively entrained to parkinsonian beta oscillations. *Journal of Neuroscience*, 37(41), 9977–9998.

Authors: I. Carannante, M. Scolamiero, J.J.J. Hjorth, A. Kozlov, B. Bekkouche, L. Guo, A. Kumar, W. Chacholski and J. Hellgren Kortaleski

- 695 Shen, W., Zhai, S., & Surmeier, D. J. (2022). Striatal synaptic adaptations in parkinson's disease. *Neurobiology of Disease*,  
696 167, 105686.
- 697 Singh, A., Mewes, K., Gross, R. E., DeLong, M. R., Obeso, J. A., & Papa, S. M. (2016). Human striatal recordings reveal  
698 abnormal discharge of projection neurons in parkinson's disease. *Proceedings of the National Academy of Sciences*,  
699 113(34), 9629–9634.
- 700 Strafella, A. P., Paus, T., Barrett, J., & Dagher, A. (2001). Repetitive transcranial magnetic stimulation of the human  
701 prefrontal cortex induces dopamine release in the caudate nucleus. *The Journal of neuroscience*, 21(15), RC157.
- 702 Suarez, L. M., Solis, O., Sanz-Magro, A., Alberquilla, S., & Moratalla, R. (2020). Dopamine d1 receptors regulate spines in  
703 striatal direct-pathway and indirect-pathway neurons. *Movement Disorders*, 35(10), 1810–1821.
- 704 Surmeier, D. J., Graves, S. M., & Shen, W. (2014). Dopaminergic modulation of striatal networks in health and parkinson's  
705 disease. *Current opinion in neurobiology*, 29, 109–117.
- 706 Tachibana, Y., Iwamuro, H., Kita, H., Takada, M., & Nambu, A. (2011). Subthalamo-pallidal interactions underlying  
707 parkinsonian neuronal oscillations in the primate basal ganglia. *European Journal of Neuroscience*, 34(9), 1470–1484.
- 708 Tanimura, A., Du, Y., Kondapalli, J., Wokosin, D. L., & Surmeier, D. J. (2019). Cholinergic interneurons amplify  
709 thalamostriatal excitation of striatal indirect pathway neurons in parkinson's disease models. *Neuron*, 101(3), 444–458.
- 710 Taverna, S., Ilijic, E., & Surmeier, D. J. (2008). Recurrent collateral connections of striatal medium spiny neurons are  
711 disrupted in models of parkinson's disease. *Journal of Neuroscience*, 28(21), 5504–5512.
- 712 Underwood, C. F., & Parr-Brownlie, L. C. (2021). Primary motor cortex in parkinson's disease: Functional changes and  
713 opportunities for neurostimulation. *Neurobiology of Disease*, 147, 105159.
- 714 Valsky, D., Heiman Grosberg, S., Israel, Z., Boraud, T., Bergman, H., & Deffains, M. (2020). What is the true discharge rate  
715 and pattern of the striatal projection neurons in parkinson's disease and dystonia? *Elife*, 9, e57445.
- 716 Van Geit, W., Gevaert, M., Chindemi, G., Rössert, C., Courcol, J.-D., Muller, E. B., ... Markram, H. (2016). Bluepyopt:  
717 leveraging open source software and cloud infrastructure to optimise model parameters in neuroscience. *Frontiers in  
718 neuroinformatics*, 10, 17.

- 719 Viaro, R., Morari, M., & Franchi, G. (2011). Progressive motor cortex functional reorganization following  
720 6-hydroxydopamine lesioning in rats. *Journal of Neuroscience*, 31(12), 4544–4554.
- 721 Wall, N. R., De La Parra, M., Callaway, E. M., & Kreitzer, A. C. (2013). Differential innervation of direct-and  
722 indirect-pathway striatal projection neurons. *Neuron*, 79(2), 347–360.
- 723 Zaja-Milatovic, S., Milatovic, D., Schantz, A., Zhang, J., Montine, K., Samii, A., ... Montine, T. (2005). Dendritic  
724 degeneration in neostriatal medium spiny neurons in parkinson disease. *Neurology*, 64(3), 545–547.
- 725 Zhai, S., Shen, W., Graves, S. M., & Surmeier, D. J. (2019). Dopaminergic modulation of striatal function and parkinson's  
726 disease. *Journal of Neural Transmission*, 126, 411–422.
- 727 Ztaou, S., & Amalric, M. (2019). Contribution of cholinergic interneurons to striatal pathophysiology in parkinson's  
728 disease. *Neurochemistry international*, 126, 1–10.

## TECHNICAL TERMS

- 729 **Snudda:** software tool for generating network connectivity based on single-cell morphologies. Uses  
730 NEURON to simulate the resulting networks.
- 731 **treem:** neuron morphology processing tool which provides data structure and command-line tools for  
732 accessing and manipulating the digital reconstructions of the neuron morphology in  
733 Stockley-Wheal-Cannon format (SWC).
- 734 **Directed clique:** a set of vertices in a directed graph which are pairwise connected (not necessarily  
735 reciprocally) and there exists a unique source and a unique sink among them.